AIR-BEARING TESTBED OF SPACECRAFT FORMATION: SYSTEM DESCRIPTION AND EXPERIMENTS

CHIHANG YANG[1], HAO ZHANG[2], WEICHAO ZHONG[3]

Abstract. Via cooperation among multiple spacecraft, spacecraft formations can enable many near Earth and deep-space missions with low cost but high robustness. Controlling spacecraft formations is more complicated than that of traditional monolithic spacecraft. Control algorithms must be sufficiently tested and validated on ground. Hence on-ground facility that provides micro-gravity environment are indispensable. This work presents the on-ground formation flight testbed in Technology and Engineering Center for Space Utilization, Chinese Academy of Sciences. The testbed is consisted of a highly-flat granite surface, four air-bearing robots, and a camera-based motion measurement subsystem. Each robot can move frictionlessly on the granite surface with three degree of freedoms, including two translational and one rotational degree of freedoms. Each robot is controlled by four carefully-calibrated fans. Several test experiments shows that centimeter-level position control accuracy and less-than-one-degree-level attitude control accuracy can be achieved. A tight formation control experiment with sophisticated scenario demonstrates that the air-bearing testbed is scalable, and capable of testing multi-spacecraft control algorithms.

Key words: air-bearing robots, spacecraft formations, on-ground micro-gravity facility, formation control, collision avoidance.

1. INTRODUCTION

As an emerging form of space missions, spacecraft formations are capable of performing complicated space missions. Compared with traditional monolithic satellites, spacecraft formations are more robust and usually have lower costs. Small formation scale and high-precision control are required by many spacecraft formation-flying missions, such as synthetic aperture telescope [1], Interferometric SAR [2], and on-orbit assembly [3]. The formation scales of different missions vary from several meters to hundreds of meters, and the required control accuracy is usually from dozens of centimeters to several millimeters.

Controlling a satellite formation, especially in close proximity, is a challenging task. The control framework should address many different aspects, such as collision

[1]University of Chinese Academy of Sciences, Beijing 100049, China

[2]Key Laboratory of Space Utilization, Technology and Engineer Center for Space Utilization, Chinese Academy of Sciences, Beijing 100094, China; hao.zhang.zhr@gmail.com

[3]Shanghai Institute of Satellite Engineering, Shanghai 201109, China

avoidance, adding or removing new members, simple actuators, limited sense capability, etc. In addition, it is also desired that the control be performed in realtime. To verify the effectiveness and decrease the risk of the mission, it is necessary to test the control algorithm in a on-ground facility that can provide micro-gravity environment.

There is a variety of ways to achieve a micro-gravity environment, such as aircraft parabolic flights, drop towers, weight-reducing suspension systems, and underwater test facilities [4]. Aircraft parabolic flights and drop towers can provide three-dimensional micro-gravity environment yet with only several or tens of seconds [5, 6]. The duration time is too short to perform formation control experiments, which usually last for several orbital periods. Weight-reducing suspension systems and underwater tests can achieve long duration time of micro-gravity environment. However, the former constrains the movement of tested devices badly [7], and the latter brings high resistance due to the medium [8].

Planar air-bearing testbed are another type of micro-gravity platform. The spacecraft are simulated by air-bearing robots. Each robot is mounted on several air bearings that allow for almost frictionless motion on a flat surface. In this way, air-bearing testbed can offer a two-dimensional micro-gravity environment with 10^{-3}-$10^{-5}g$ (where g is the Earth's gravitational acceleration) of residual gravity acceleration [4]. The duration time is usually as long as dozens of minutes. Therefore, planar air-bearing testbed are suitable to perform the formation-flying experiments.

There are many investigators that have simulated the formation-flying experiments based on the planar air-bearing platform. In the end of 1990s, Robertson et al. tested the control strategy of the three spacecraft formation of Orion mission [9]. In 2005, a planar air-bearing testbed called SPHERES (Synchronized Position Hold Engage Re-orient Experimental Satellites) program was developed at the Massachusetts Institute of Technology [10]. This program supported the control algorithms verification of multiple formation-flying missions, including TechSat 21 and Space Technology 3. The on-orbit assembly was simulated using four air-bearing robots by Bevilacqua et al. in 2011 [11]. Guglieri et al. performed a rendezvous and docking experiment in 2014 [12]. In 2019, Rughani et al. tested the proximity operations between three spacecraft using air-bearing testbed [13].

The air-bearing testbed is mainly composed of a flat surface and air-bearing robots. To maintain the micrometer-level air cushion between robots' feet and flat surface, the flat surface should be extremely flat, which gives high requirements to its material. There are three kinds of material usually used to construct the surface: granite, glass, and epoxy. The maximum size of the glass surface is usually smaller than $4\,\mathrm{m}^2$ due to the limitation of the production technology [14, 15]. The surface made by epoxy have unlimited size but have worse quality [16, 17]. Hence, the most popular material is granite because of its high flatness, small roughness, and modest size [18, 19, 20]. The flat surface of the air-bearing testbed in this paper is constructed by granite.

The motion sensors and actuators of the air-bearing robots are two key elements of the control loop. To measure the position and attitude of the robots, several kinds of sensors have been applied. In some proximity operation experiments, several cameras are mounted on the side of robots to sensor other robots, thus directly provide the relative position and attitude [21, 22]. However, side cameras has limited visions and needs heavy on-board computation. A more popular way is to mount one or more cameras on the overhead to measure the motion of each robot as a global sensor [23, 24]. Besides, pseudo-GPS indoor system is applied in some testbed [25]. In comparison, the overhead cameras has much lower costs. In this paper, the positions and attitudes are measured by an overhead infrared camera.

To simulate the actuators of the spacecraft, thrusters are usually adopted to control the air-bearing robots. As the robot has three degree of freedoms, three or more counter facing pairs of thrusters are offen equipped with evenly spacing [26, 27]. Also, there are some air-bearing robots of which thrusters mounted with specific configuration [28, 29]. The maximum force of single thrusters are usually from dozens of milinewton to a few Newtons [30, 31]. However, the thrusters continuously consume the limited high-pressure air in the tank which supplies the air bearings at the same time to achieve frictionless motion. Hence, the thrusters will reduce the duration time of the air-bearing robots. On the other hand, most thrusters are custom-made, which increases the difficulties of debugging and maintenance. To avoid these issues, a fan propulsion system is adopted to control the air-bearing robots. And the fan propulsion system is completely based on commercial equipments, which reduce the costs and difficulties of maintenance.

In this paper, the air-bearing testbed is introduced first. To achieve high-precision control, the control model of the air-bearing robots is built with parameters measured. Based on the PID (proportional–integral–derivative) controller, the subcentimeter position precision is obtained during the single air-bearing control experiment. Finally, an formation-flying experiment with four air-bearing robots is performed with the artificial potential field (APF) method.

2. SYSTEM DESCRIPTION

The schematic diagram of the air-bearing simulator is shown in Fig. 1. There are four air-bearing robots floating on a 4×3-m^2 granite surface. The infrared camera takes images of the distribution of each robot on the granite surface with a 10-Hz frequency. The positions and attitudes of robots can be obtained after processing the image data from infrared camera. A photo of the testbed is shown in Fig. 2.

As illustrated by Fig. 3, the air-bearing robot is three-tiered-structured. The air-bearing subsystem is installed on the bottom tier, including the high-pressure air passage, air reducers, and three air bearings. The air tank is located in the center of the robot. The air-bearing subsystem can support the robots working more than one hour. The middle tier contains the power subsystem and the attitude and position control

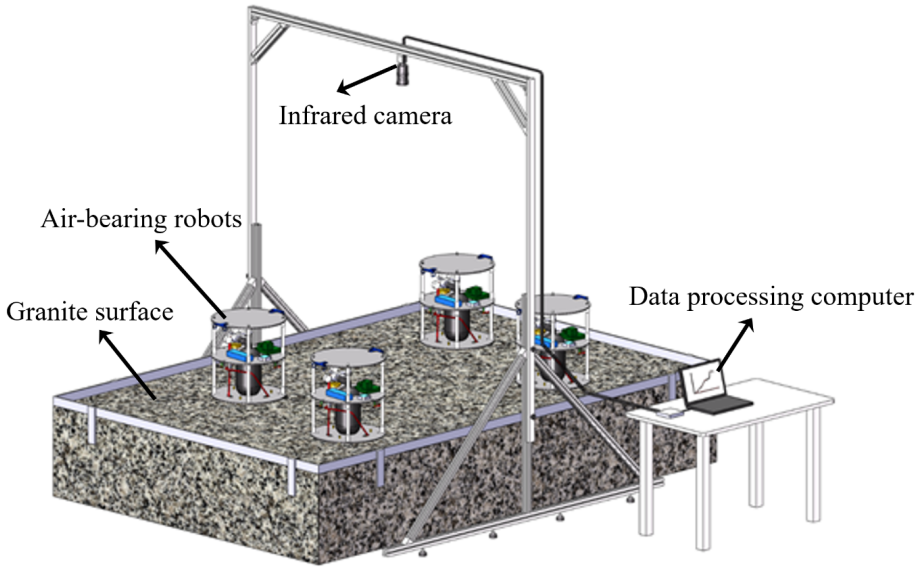

Fig. 1 – Schematic diagram of the air-bearing testbed.

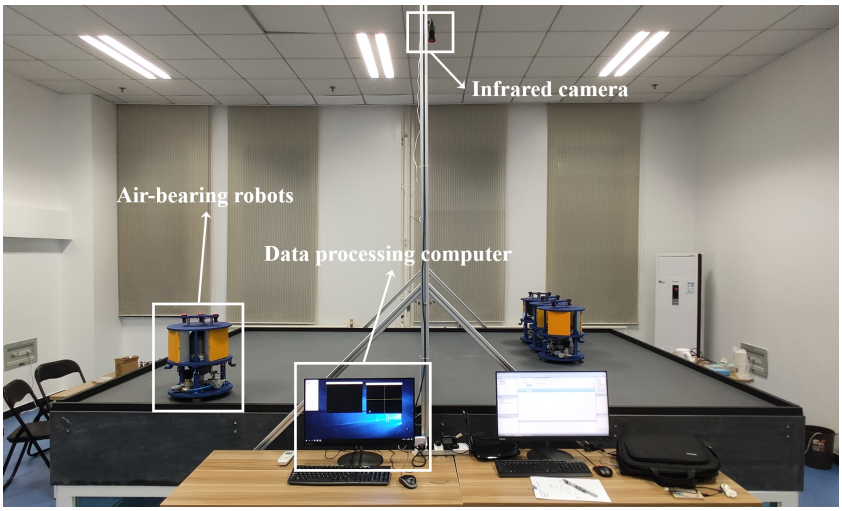

Fig. 2 – Photo of the air-bearing testbed.

subsystem. The attitude and position control subsystem consists of four propulsion fans, an on-board computer, and a wireless module to receive attitude and position information from the data processing computer. On the top tier, there are three sign lights to determine the attitude and position of the robot. To be identified, each robot has a unique distribution of sign lights. Besides, some mounting holes are reserved on the top tier for equipments that may be used in the future, such as cameras or lidars.

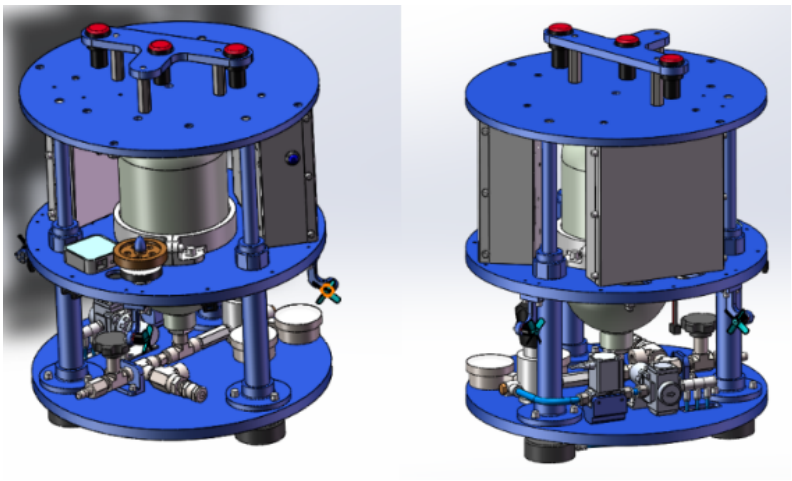

Fig. 3 – Model of air-bearing robot.

3. THE CONTROL MODEL OF AIR-BEARING ROBOTS

3.1. The control model

To achieve high-precision control of the air-bearing robots, the control model is built in this section, including the translational model and the rotational model. The motion and rotation of the robots are described in a two-dimensional inertial coordinate system I shown in Fig. 4: the origin O_I is located at the geometrical center of the granite surface; y_I-axis is along the short side of the granite surface with an opposite direction to the data processing computer; and x_I-axis is determined by a right-handed coordinate system.

As illustrated in Fig. 5, the air-bearing robot is driven by two pairs of propulsion fans. Four fans are numbered counterclockwise. The directions of propulsion forces remain fixed in the robot-fixed coordinate system L: the Origin O_L is located in the geometrical center of the robot; x_L-axis points to the second sign light; and y_L-axis points to the third sign light.

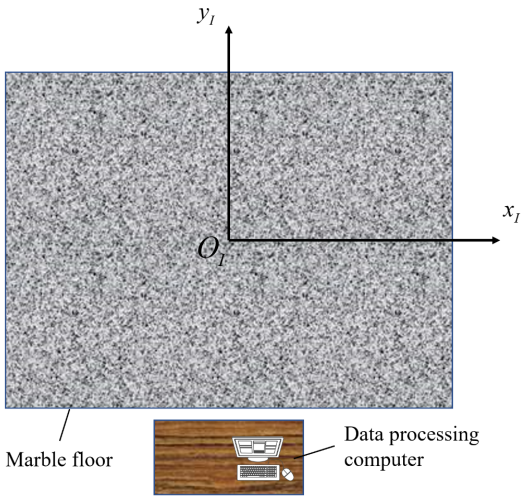

Fig. 4 – Inertial coordinate system.

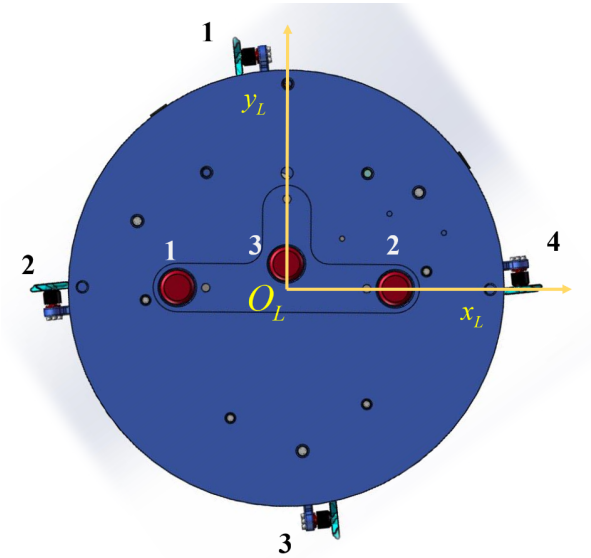

Fig. 5 – Robot-body-fixed frame.

The translational control model can be defined as follows:

$$m\mathbf{a} = \sum_{i=1}^{4} \mathbf{M}(\beta)\mathbf{F}_i \tag{1}$$

where m is the mass of the air-bearing robot, $\mathbf{a}$ is the acceleration in the inertial coordinate, $\mathbf{F}_i$ is the propulsion force of ith fan in the robot-fixed coordinate, and $\mathbf{M}(\beta)$ is the transformation matrix from the inertial coordinate to the robot-fixed coordinate:

$$\mathbf{M}(\beta) = \begin{bmatrix} \cos(\beta) & -\sin(\beta) \\ \sin(\beta) & \cos(\beta) \end{bmatrix} \tag{2}$$

Here, β is the attitude angle of the robot, which is defined as the clockwise rotation angle from x_L-axis to x_I-axis.

The rotation control model is as follows:

$$J\alpha = \sum_{i=1}^{4} \mathbf{L}_i{}^T \mathbf{F}_i \tag{3}$$

where J is the moment of inertia of the robot, α is the angular acceleration, and $\mathbf{L}_i$ is the lever arm of $\mathbf{F}_i$ relative to the center of mass of the robot.

3.2. Measurement and calibration

There are several parameters in the control model to be measured, including the mass m, the moment of inertia J, and the coordinate of the center of mass $\mathbf{P}_{\text{bc}}$ in robot-fixed frame. Besides, the propulsion force needs to be calibrated.

3.2.1. Measurement of parameters

The parameters of two different air-bearing robots are measured. Results are shown in Table 1.

Table 1
Parameters of Air-bearing robots

	Air-bearing robot 1	Air-bearing robot 2
m [kg]	17.665	17.486
J [kg/m^2]	0.259586	0.255583
$\mathbf{P}_{\text{bc}}$ [cm]	[-0.934, 0.052]	[-1.492, 0.042]

It can be seen that the differences of masses and moments of inertia between two robots are below 2%. Compared with the 40-cm diameter of robots, the position of the barycenter, that is the offset relative to the geometric center, is relatively little. These differences are mainly due to the different distributions of sign lights and mass of air on the tank, both of which just have a slight effect on the control accuracy. Then, lever arms of four propulsion fans can be calculated based on the 3D model of the robots. In this way, the control model is obtained.

3.2.2. Calibration of propulsion fan

The propulsion force of four identical fans are directly controlled by the duty cycle of pulse-width modulation (PWM) signals. To acquire accurate control force, the correspondence relationship between the output force and the duty cycle of PWM control signal is calibrated. As shown in Fig. 6, the equipment measuring propulsion force consist of a microcontroller, an one-to-one transmission lever, and a force sensor with 1 mN precision.

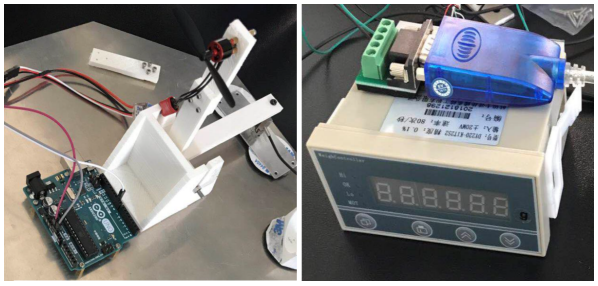

Fig. 6 – The equipment measuring propulsion force.

During the calibration, the rotational speed of the propulsion fan is decided by the PWM signal produced by the microcontroller controls. The output forces are measured by the force sensor. The calibrating results are illustrated in Fig. 7. The correspondence relationship is strongly nonlinear. The maximum propulsion force is around 250 mN. To obtain accurate output forces, the saturation force is set as 150 mN during the control. Since the mass of each air-bearing robot is around 17.5 kg, the maximum control acceleration is around 12 mm/s^2, which is enough to control the air-bearing robot in the frictionless environment.

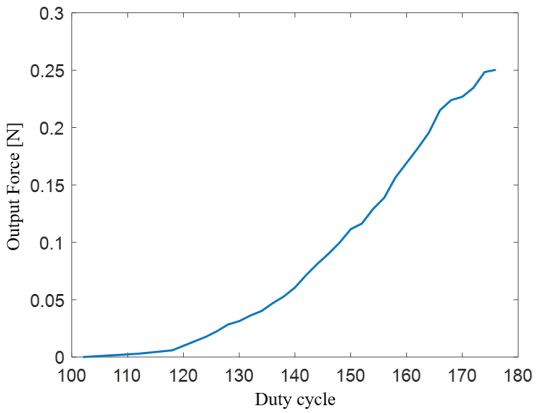

Fig. 7 – The correspondence relationship between the output force and the duty cycle of PWM control signal.

3.2.3. Allocation of propulsion forces

To control the translation and rotation of the robot, the translational control force $\mathbf{F}$ and the control torque T should be produced by appropriate allocation of propulsion forces of four fans.

According to Fig. 8, the point of applications $\mathbf{P}_i$ and propulsion directions $\mathbf{D}_i$ are as follows in the robot-fixed coordinate:

$$\begin{cases} \mathbf{P}_1 = \mathbf{M}(\delta)\ [0,R]^T \\ \mathbf{P}_2 = \mathbf{M}(\delta)\ [-R,0]^T \\ \mathbf{P}_3 = \mathbf{M}(\delta)\ [0,-R]^T \\ \mathbf{P}_4 = \mathbf{M}(\delta)\ [R,0]^T \end{cases}, \quad \begin{cases} \mathbf{D}_1 = \mathbf{M}(\delta)\ [1,0]^T \\ \mathbf{D}_2 = \mathbf{M}(\delta)\ [0,-1]^T \\ \mathbf{D}_3 = \mathbf{M}(\delta)\ [-1,0]^T \\ \mathbf{D}_4 = \mathbf{M}(\delta)\ [0,1]^T \end{cases} \tag{4}$$

where R is the radius of the robot, and $\mathbf{P}_i$ and $\mathbf{D}_i$ satisfy

$$\begin{aligned} \mathbf{F}_i &= \mathbf{D}_i F_i \\ \mathbf{L}_i &= \mathbf{P}_i - \mathbf{P}_{bc} \end{aligned}. \tag{5}$$

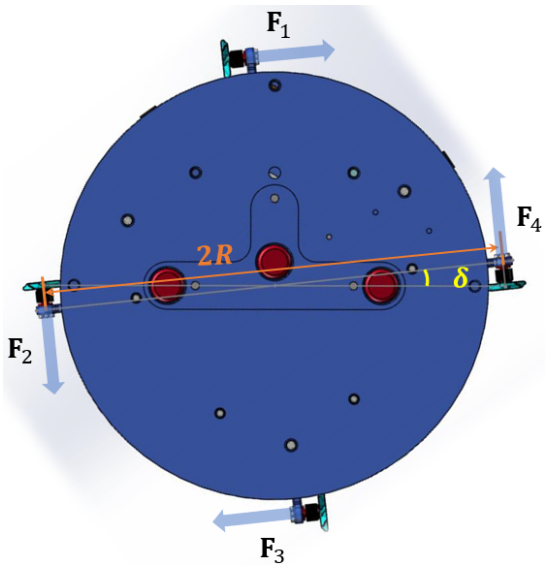

Fig. 8 – The installation configuration of propulsion fans.

Substitute Eq.(5) into Eqs.(1) and (3), there are

$$\begin{aligned} \mathbf{M}(\theta)^T \mathbf{F} &= \sum_{i=1}^{4} \mathbf{D}_i F_i \\ T &= \sum_{i=1}^{4} (\mathbf{P}_i - \mathbf{P}_{bc})^T \mathbf{D}_i F_i \ . \end{aligned} \tag{6}$$

The desired translational control force $\mathbf{F}$ and the control torque T is decided by the

control law. And the force of each fan, that is F_i, is calculated by solving Eq.6 with least square method. According to calibrating results of the propulsion fan, the duty cycle of PWM control signal for F_i is obtained. In this way, specific desired control force and torque can be produced by four propulsion fans.

4. CONTROL OF SINGLE AIR-BEARING ROBOT

4.1. Preliminary Control Setting

In order to test the performance of the air-bearing formation flight simulation system, several testcase control experiments can designed. In the current setting, the position control and attitude control of single air-bearing robot are based on the classical PID control. The control diagram is shown as follows:

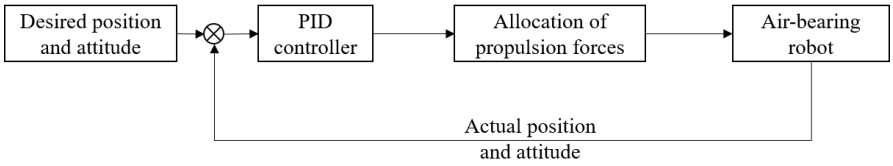

Fig. 9 – Control diagram of single air-bearing robot control experiment.

As one of the most popular controllers, PID controller is composed of three terms:

$$u = K_P e + K_I \int_{\tau=0}^{t} e \, d\tau + K_D \dot{e} \tag{7}$$

where e is the error between desired state and actual state, and K_P, K_I and K_D are the coefficients of proportional term, integral term, and derivative term, respectively. The error is mainly reduced by the proportional term. The derivative term can estimate the future trend of the error, thus can accelerate convergence. However, it will increase the high-frequency compounds of errors, which is inescapable as random noise is common in physical systems. The integral term can eliminate the steady-state error but may degrade the stability of the system.

4.2. Control experiment

In fact, PD (proportional-derivative) controller is able to achieve quick response and eliminate the overshoot. However, the steady-state error still exists under the PD control. The integral term can eliminate the steady-state error but will decelerate the convergence. An error threshold is set to limit the integral term, which means the integral term only works when the error is smaller than a threshold value. As the derivative term will increase the high-frequency compounds, moving average filters are used to mitigate the effect of random noise. Besides, the control force of each fan is limited below 0.15 N.

Two experiments that involve only one robot are performed. The aim of these experiments is to examine a single robot's control response, such as the control accuracy. The control objective of first experiment is to drive the robot to a fixed point and to maintain a stationary attitude. In the second experiment, the robot is driven to track a circular trajectory.

4.3. Fixed point experiment

Initially, the air-bearing robot is set on the origin and the attitude is set as 0°. And the target states are as follows:

$$\begin{aligned} x_I &= 1000\,\text{mm} \\ y_I &= 1000\,\text{mm} \\ \theta_d &= 120^\circ. \end{aligned} \tag{8}$$

To reduce the difficulty of coefficient tuning, a numerical scenario is created based on the control model and the calibration results in Section 3. On the basis of control coefficients in the numerical simulation, the coefficient tuning in the experiment can be easily done after slightly adjustment. This means the control model and calibration of propulsion fan are accurate enough.

The control results are illustrated in Fig.10. The slight variations of states are due to the random noise. The precision of position control and attitude control is below 0.5 cm and 0.5°, respectively.

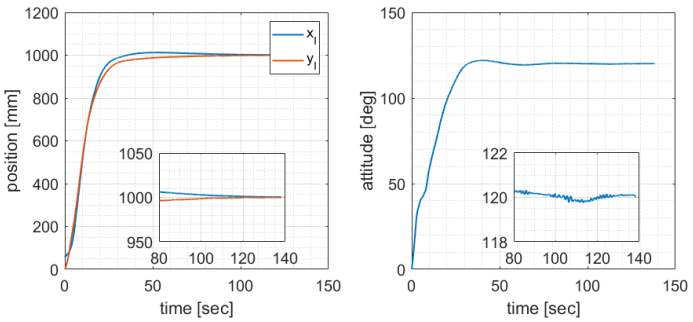

Fig. 10 – Results of single air-bearing robot control experiment.

The control process is shown in Fig.11 with several snapshots. It should be noticed that three air-bearing robots in the bottom left do not participate the control and remain static during the control process. The controlled robot arrived the target position finally.

4.4. Trajectory tracking experiment

In the trajectory tracking experiment, the target spins around a circle with a 110-sec period and a 100-cm diameter. And the target attitude is constantly set as 0°.

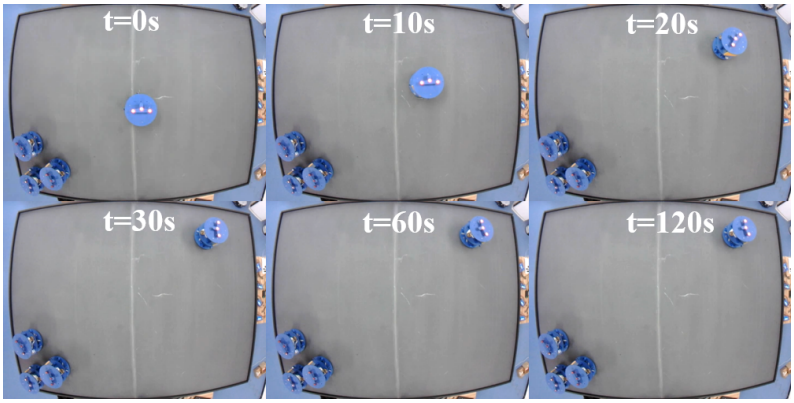

Fig. 11 – Control process of single air-bearing robot control experiment.

The PID controller is also adopted in this experiment. Initially, the robot is far away from the target trajectory. As shown in the left subplot in Fig.12, the robot is gradually close to the target and follows the trajectory finally. As the target is constantly moving, there is a near constant distance between the target and the robot as shown in the right subplot in Fig.12. Once the trajectory tracking is achieved, the fluctuation of the distance is below 3 cm. Therefore, the trajectory tracking experiment is accomplished with centimeter-level precision.

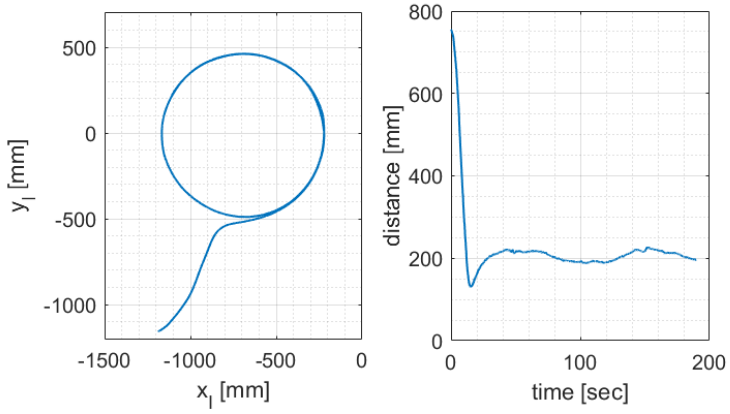

Fig. 12 – Control results of trajectory tracking experiment.

5. TIGHT FORMATION CONTROL OF AIR-BEARING ROBOTS

This section considers a more complicated experiment with multiple air-bearing robots. Four air-bearing robots are desired to construct a dynamic configuration. The cooperations between robots and collision avoidance technique are tested.

5.1. Artificial potential field method

In the formation control, the attitude of each robot is controlled by the PID controller. The APF method is adopted to control the positions of robots, and furthermore achieves the configuration initialization and configuration maintenance. The positions are controlled by the APF method. The formation control diagram is shown in Fig.13. As the translational model is second-order, a double-loop control is adopted. The outer position–velocity loop is controlled by APF method, which produced the desired velocity based on the distribution of robots. For each robot, the Q-guidance law tracks the desired velocity of the method and accomplish the inner velocity–acceleration loop.

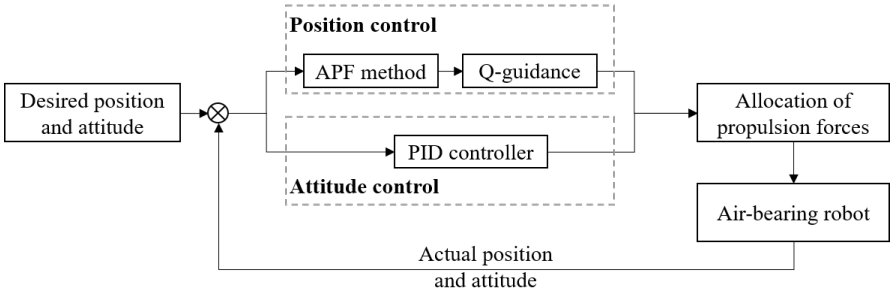

Fig. 13 – Formation control diagram of air-bearing robots.

By combining several artificial potential fields, the APF method can control robots achieve the target distribution without collision. The APF method is robust and can dynamically switch the target of each robots during control. For *i*th air-bearing robot, the desired velocity is as follows:

$$\mathbf{v}_i = \mathbf{v}_i^{Gather} + \mathbf{v}_i^{Dock} + \mathbf{v}_i^{Avoid} \tag{9}$$

where $\mathbf{v}_i^{Gather}$, $\mathbf{v}_i^{Dock}$, and $\mathbf{v}_i^{Avoid}$ are artificial potential fields of three types of behaviours as follows [32]:

$$\begin{aligned}
\mathbf{v}_i^{Gather} &= \sum_{j=1}^{4} c_i \left(\xi_j - \mathbf{x}_i\right) \\
\mathbf{v}_i^{Dock} &= \sum_{j=1}^{4} d_i \exp\left(-\frac{\left\|\xi_j - \mathbf{x}_i\right\|^2}{k_{d,i}}\right)\left(\xi_j - \mathbf{x}_i\right) \\
\mathbf{v}_i^{Avoid} &= \sum_{j=1}^{4} -b_i \exp\left(-\frac{\left\|\mathbf{x}_j - \mathbf{x}_i\right\|^2}{k_{a,i}}\right)\left(\mathbf{x}_j - \mathbf{x}_i\right)
\end{aligned} \tag{10}$$

where $\mathbf{x}_i$ and ξ_j are the positions of the *i*th robot and the *j*th target position, respectively. And c_i, d_i, $k_{d,i}$, b_i, and $k_{a,i}$ are parameters to adjust the magnitude or range of the corresponding behaviour. The velocity fields of three behaviours are illustrated in Fig.14. The gather behavior drive the robots move towards the target and has a

global effect. The dock behavior is local and only works when the robot is nearby some target. It leads to a smooth docking. And the avoid behavior can prevent two robots collide with each other. The formation control with collision avoidance can be accomplished by the combination of these behaviors.

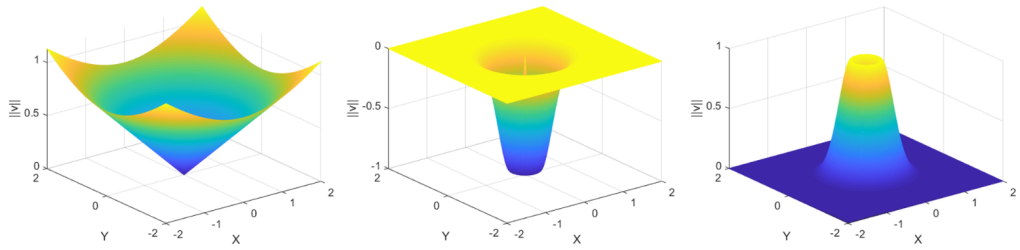

(a) gather behavior (b) dock behavior (c) avoid behavior

Fig. 14 – Artificial potential fields of three behaviors.

5.2. Control experiment

Initially, four air-bearing robots are randomly distributed in the plane. The final target formation is a square that spins around a circle. The attitude of each robot is set as 0° constantly. The scenario has two stages:

(1) Initially three robots form a group and the fourth robot serves as an intruder. Thus the group should accomplish the formation configuration while avoiding the fourth one.

(2) The fourth one becomes a new member and is to be added into the formation.

The trajectory evolutions are shown in Fig.15. Several snapshots of the control process are illustrated in Fig.16. The robots are distributed to the moving target points finally. Due to the avoid behavior and adaptive target switches, the trajectories are relatively complicated. Consider the 400-mm diameter of robots, the collision threshold is set as 500 mm, which is illustrated as the red line in Fig.17. The blue curve in Fig.17 is the minimum distance between any two of robots. As can be seen, the minimum distance is always above the collision threshold.

6. CONCLUSION

In this paper, an air-bearing testbed using fan propulsion system is presented. The system includes multiple air-bearing robots and hence can simulate space missions with one or more satellites in a planar micro-gravity environment. This system supports experiment with long duration, from tens of minutes to couples of hours. The control precision of the robots can reach sub-centimeter level for position control and sub-degree level for attitude control. This testbed is used in a formation

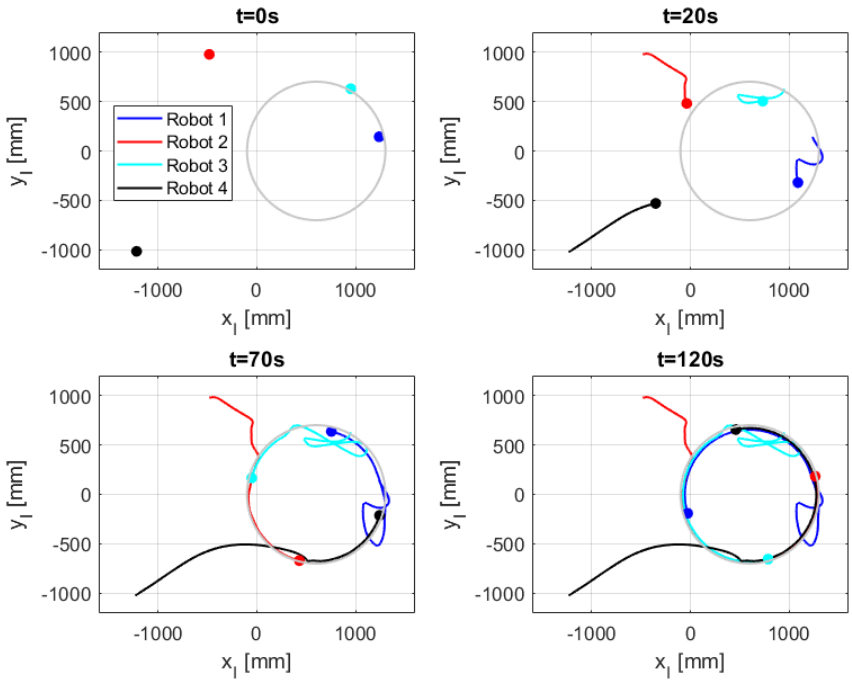

Fig. 15 – Trajectory evolutions in formation control experiment.

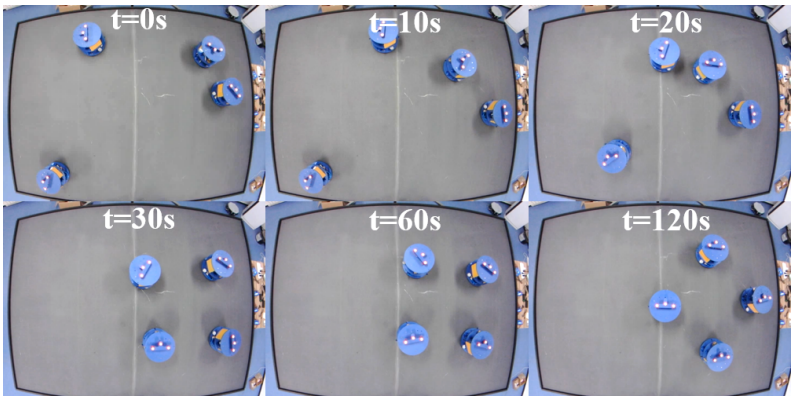

Fig. 16 – Control process of formation control experiment.

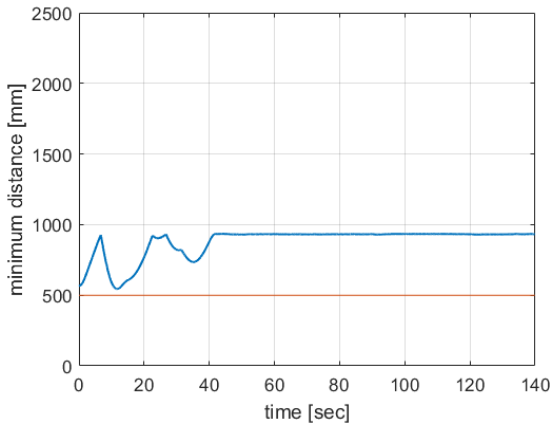

Fig. 17 – Minimum distance in formation control experiment.

control experiment involving formation acquisition, collision avoidance and formation reconfiguration. Result demonstrates its capability of validating algorithms for sophisticated spacecraft formations.

The air-bearing testbed is extensible. It can be further used in other scenarios, for example, validating GNC algorithm for space rendezvous, testing drag-free control algorithms for distributed optical interferometers.

Received on December 2020

REFERENCES

1. BUINHAS, L., PHILIPS-BLUM, M., FRANKL, K., PANY, T., EISSFELLER, B., FÖRSTNER, R., *Formation operations and navigation concept overview for the IRASSI space interferometer*, 2018 IEEE Aerospace Conference, pp. 1–16, 2018.
2. KRIEGER, G., HAJNSEK, I., PAPATHANASSIOU, K.P., YOUNIS, M., MOREIRA, A., *Interferometric synthetic aperture radar (sar) missions employing formation flying*, Proceedings of the IEEE, **98**, *5*, pp. 816–843, 2010.
3. SHE, Y., LI, S., WANG, Z., *Constructing a large antenna reflector via spacecraft formation flying and reconfiguration control*, Journal of Guidance, Control, and Dynamics, **42**, *6*, pp. 1372–1382, 2019.
4. RYBUS, T. SEWERYN, K., *Planar air-bearing microgravity simulators: Review of applications, existing solutions and design parameters*, Acta Astronautica, **120**, pp. 239–259, 2016.
5. PLETSER, V., *European aircraft parabolic flights for microgravity research, applications and exploration: A review*, REACH, **1**, pp. 11–19, 2016.
6. KÖNEMANN, T., KACZMARCZIK, U., GIERSE, A., GREIF, A., LUTZ, T., MAWN, S., SIEMER, J., EIGENBROD, C., VON KAMPEN, P., LÄMMERZAHL, C., *Concept for a next generation drop tower system*, Advances in Space Research, **55**, *6*, pp. 1728–1733, 2015.
7. BROWN, H.B., DOLAN, J.M., *A novel gravity compensation system for space robots*, Proceedings of the ASCE Specialty Conference on Robotics for Challenging Environments, 1994.

8. WHITACRE, W., *An autonomous underwater vehicle as a spacecraft attitude control simulator*, 43rd AIAA Aerospace Sciences Meeting and Exhibit, Reno, USA, 2005.

9. ROBERTSON, A., INALHAN, G., HOW, J., *Spacecraft formation flying control design for the orion mission*, Guidance, Navigation, and Control Conference and Exhibit, p. 4266, 1999.

10. SAENZ-OTERO, A., MILLER, D.W., *SPHERES: a platform for formation-flight research*, in: *"UV/Optical/IR Space Telescopes: Innovative Technologies and Concepts II"* (ed. H.A. MacEwen), Vol. 5899, pp. 230–240, International Society for Optics and Photonics, SPIE, 2005.

11. BEVILACQUA, R., ROMANO, M., CURTI, F., CAPRARI, A.P., PELLEGRINI, V., *Guidance navigation and control for autonomous multiple spacecraft assembly: analysis and experimentation*, International Journal of Aerospace Engineering, article ID 308245, 2011.

12. GUGLIERI, G., MAROGLIO, F., PELLEGRINO, P., TORRE, L., *Design and development of guidance navigation and control algorithms for spacecraft rendezvous and docking experimentation*, Acta Astronautica, **94**, *1*, pp. 395–408, 2014.

13. RUGHANI, R., VILLAFANA, L., BARNHART, D.A., *Swarm RPO and docking simulation on a 3dof air bearing platform*, 70th International Astronautical Congress (IAC), Washington DC, United States, pp. 21–25, 2019.

14. YOSHIDA K., UMETANI, Y., *Control of space free-flying robot*, Proceedings of the 29th Conference on Decision and Control, Vol. 1, pp. 97–102, Honolulu, Hawaii, 1990.

15. BINDEL, D., ZARAMENSKIKH, I., IVANOV, D., OVCHINNIKOV, M.Y., PRONCHEVA, N., *A laboratory facility for verification of control algorithms for a group of satellites*, Journal of Computer and Systems Sciences International, **48**, *5*, p. 779, 2009.

16. HALL, J.S., ROMANO, M., MILELLA, A., DI PAOLA, D., CICIRELLI, G. , *Laboratory experimentation of guidance and control of spacecraft during on-orbit proximity maneuvers*, in: *"Mechatronic systems simulation modeling and control"* (eds. A. Milella, D. Di Paola, G. Cicirelli), pp. 187–225, InTech, 2010.

17. SAULNIER, K., PEREZ, D., TILTON, G., GALLARDO, D., SHAKE, C., HUANG, R., BEVILACQUA, R., *Operational capabilities of a six degrees of freedom spacecraft simulator*, Proceedings of the AIAA Guidance, navigation, and control (GNC) conference (AIAA-GNC'2013), p. 5253, Boston, USA, 2013.

18. PAPADOPOULOS, E., PARASKEVAS, I.S., FLESSA, T., NANOS, K., REKLEITIS, G., KONTOLATIS, I., *The NTUA space robot simulator: Design & results*, Proceedings of 10th ESA Workshop on Advanced Space Technologies for Robotics and Automation (ASTRA'2008), Noordwijk, The Netherlands, ESTEC, 2008.

19. SCHLOTTERER, M., THEIL, S., *Testbed for on-orbit servicing and formation flying dynamics emulation*, Proceedings of the AIAA Guidance, Navigation and Control Conference (AIAA-GNC'2010), p. 8108, Toronto, Canada, 2010.

20. RYBUS, T., BARCIŃSKI, T., LISOWSKI, J., NICOLAU-KUKLIŃSKI, J., SEWERYN, K., CIESIELSKA, M., GRASSMANN, K., GRYGORCZUK, J., KARCZEWSKI, M., KOWALSKI, M., et al., *New planar air-bearing microgravity simulator for verification of space robotics numerical simulations and control algorithms*, Proceedings of 12th Symposium on Advanced Space Technologies in Robotics and Automation, Noordwijk, The Netherlands, ESTEC, 2013.

21. JIGALIN, A., GURFIL, P., *Investigation of multiple-baseline stereovision for state estimation of unknown dynamic space targets*, Proceedings of the Institution of Mechanical Engineers, Part G: Journal of Aerospace Engineering, **230**, *2*, pp. 207–233, 2016.

22. SHTARK, T., GURFIL, P., *Tracking a non-cooperative target using real-time stereovision-based control: an experimental study*, Sensors, **17**, *4*, p. 735, 2017.

23. PAYO, I., RAMOS, F., CORTÁZAR, O.D., FELIU, V., *Experimental validation of nonlinear dy-*

namic models for single-link very flexible arms, Proceedings of the 44th IEEE Conference on Decision and Control, pp. 5304–5309, Seville, Spain, 2005.

24. TSIOTRAS, P., *ASTROS: A 5dof experimental facility for research in space proximity operations*, Proceedings of the 37th AAS Guidance and Control Conference, Breckenridge, USA, 2014.
25. CURTI, F., ROMANO, M., BEVILACQUA, R., *Lyapunov-based thrusters' selection for spacecraft control: Analysis and experimentation*, Journal of Guidance, Control, and Dynamics, **33**, *4*, pp. 1143–1160, 2010.
26. FLESSA, T., PARASKEVAS, I.S., REKLEITIS, Y., PAPADOPOULOS, E., *Localization and fuel management techniques for the NTUA space servicer emulator system*, Proceeding of the 11th International Symposium on Artificial Intelligence and Robotics and Automation in Space (i-SAIRAS'2012), Turin, Italy, 2012.
27. TODA, Y., IWATA, T., MACHIDA, K., OTSUKA, A., TORIU, H., SHINOMIYA, Y. *Development of flying telerobot model for ground experiments*, The Journal of Space Technology and Science, **7**, *2*, pp. 15–22, 1991.
28. REGEHR, M.W., ACIKMESE, A.B., AHMED, A., AUNG, M., CLARK, K.C., MACNEAL, P., SHIELDS, J., SINGH, G., BAILEY, R., BUSHNELL, C., HICKE, A., LYTLE, B., RASMUSSEN, R.E., *The formation control testbed*, 2004 IEEE Aerospace Conference Proceedings (IEEE Cat. No.04TH8720), Vol. 1, pp. 557–564, Big Sky, USA, 2004.
29. SCHARF, D.P., KEIM, J.A., HADAEGH, F.Y., *Ground demonstration of synchronized formation rotations for precision, multi-spacecraft interferometers*, Proceedings of the 3rd International Symposium on Formation Flying, Missions and Technologies, 2008.
30. NEUBAUER, J., SWARTWOUT, M. , *Controlling swarms of bandit inspector spacecraft*, Proceedings of the 20th Annual AIAA/USU Conference on Small Satellites, Logan, USA, 2006.
31. MACHAIRAS, K., ANDREOU, S., PARASKEVAS, I., PAPADOPOULOS, E. , *Extending the NTUA space robot emulator for validating complex on-orbit servicing tasks*, Proceedings of the 12th Symposium on Advanced Space Technologies in Robotics and Automation (ASTRA'2013), Noordwijk, The Netherlands, 2013.
32. SCHLOTTERER, M., EDLERMAN, E., FUMENTI, F., GURFIL, P., THEIL, S., ZHANG, H., *On-ground testing of autonomous guidance for multiple satellites in a cluster*, Proceedings of the 8th International Workshop on Satellite Constellations and Formation Flying, Vol. 6, 2015.